

The Role of the $D_{13}(1520)$ Resonance in η Electroproduction

R. M. Davidson, Nilmani Mathur and Nimai C. Mukhopadhyay
Department of Physics, Applied Physics, and Astronomy
Rensselaer Polytechnic Institute
Troy, New York 12180-3590

We investigate the electroproduction of η mesons below a center of momentum energy of 1.6 GeV, with particular emphasis on the roles of the $N^*(1535)$ and $N^*(1520)$ resonances. Using the effective Lagrangian approach, we show that the transverse helicity amplitude of the $N^*(1535)$ can be extracted with good accuracy from the new eta electroproduction data, under reasonable assumptions for the strength of the longitudinal helicity amplitude. In addition, although the differential cross section is found to have a small sensitivity to the $N^*(1520)$ resonance, it is shown that a recently completed double polarization experiment is very sensitive to this resonance.

Keywords: η meson, $N^*(1520)$ and $N^*(1535)$ resonances, Polarization observables, Effective Lagrangian

PACS numbers: 13.60.Le; 12.39.-x; 12.38.Gc; 12.38.Lg

Electroexcitation of nucleon resonances (N^* states) is a clean way of studying the structures of nucleons and their excited states. Novel experimental facilities with polarized electron beams, available at accelerators like CEBAF at the Jefferson Lab (J-Lab), and corresponding developments in the polarized target technology, along with outstanding possibilities of the large solid-angle detectors (like the one in the Hall B of J-Lab), make the prospects of extracting electromagnetic amplitudes for the $N \rightarrow N^*$ excitations as functions of four-momentum transfer, Q^2 , a realistic one. Indeed, the first results of such experiments are already coming on line [1,2].

We have explored elsewhere prospects of η photoproduction as a way of studying both the $N^*(1535)$ (or S_{11}) resonance [3] and the difficult to access resonance $N^*(1520)$ [4] (or D_{13}). Moving away from the real photon point, most of our current phenomenological knowledge about the Q^2 dependence of the S_{11} and D_{13} helicity amplitudes comes from the analyses of Burkert [5] and Stoler [6]. For the S_{11} , $Q^3 A_{1/2}^s$ starts to scale at about 5 GeV², while for the D_{13} , the ratio

$$\frac{|A_{1/2}^d|^2 - |A_{3/2}^d|^2}{|A_{1/2}^d|^2 + |A_{3/2}^d|^2}$$

starts to approach unity around 3 GeV², both results in agreement with the pQCD counting rules [7]. However, the D_{13} seems to be disappearing much faster than the S_{11} with Q^2 . Thus, it is not clear that the D_{13} is, in fact, behaving according to pQCD¹ expectations, that is, it is not certain that $Q^3 A_{1/2}^d$ is scaling at these Q^2 values. Indeed, the D_{13} has never been studied at high Q^2 ($\gtrsim 3$ GeV²). As the Q^2 value at which the pQCD predictions become reliable is hotly debated in the literature [9], the exceptions to scaling should play a significant role in resolving this issue. As we will show, eta electroproduction can provide important constraints for the N- D_{13} electromagnetic transition amplitudes.

Our work should also have an impact on distinguishing among the variety of baryon models that have been discussed in the literature, starting from the old non-relativistic model [10], SU(6) analyses [11], relativized models [12], quark models involving meson and gluon exchanges between quarks [13], quark models with strong emphasis on relativity [14], models emphasizing large N_c [15], and so on. All these approaches are attempts to model QCD in the context of hadron spectroscopy. Our work here should motivate these approaches to compare with the sensitive observables coming from the new electromagnetic studies in the baryon sector.

The purpose of this Letter is to investigate the role of the D_{13} in various eta electroproduction observables. As the older data [16], taken at Bonn, DESY, and NINA, are not of good quality, the original effective Lagrangian analysis [17] did not include the D_{13} resonance. In addition, no D_{13} contribution was considered in the analysis [1] of the recent J-Lab data. Given that recent *photoproduction* data [18] are sensitive to the D_{13} , it is important to examine its role in *electroproduction*. Thus, we shall use our effective Lagrangian approach to analyze the new J-Lab data for eta

¹It should be noted that for $Q^2 \lesssim 3$ GeV², the behavior of $|A_{1/2}^d|^2/|A_{3/2}^d|^2$ can also be reproduced in constituent quark models [8].

electroproduction at Q^2 values of 2.4 and 3.6 GeV^2 . We will determine the constraints provided by these *differential cross section* data on the D_{13} helicity amplitudes, $A_{1/2}^d$, $A_{3/2}^d$ and $S_{1/2}^d$, and suggest new experiments that show greater sensitivity to these amplitudes than the current data. In particular, based on our fits to the differential cross section, we predict that a recently completed double polarization experiment at J-Lab [19] is extremely sensitive to the D_{13} helicity amplitudes. Finally, our work will provide a test of the model dependence in extracting the dominant helicity amplitude, $A_{1/2}$ of the S_{11} ($A_{1/2}^s$) from the data.

The recent J-Lab experiment [1] measured the differential cross-section for η electroproduction in the $W = \sqrt{s}$ range from 1490 MeV to 1590 MeV, and at Q^2 values of 2.4 and 3.6 GeV^2 . To a large extent, the data are independent of θ and ϕ , suggesting the dominance of the S_{11} resonance in this reaction. However, there are minor deviations from angular uniformity hinting at reaction mechanisms other than the S_{11} contribution. Taking guidance from what has been learned at the real photon point [4], we have analyzed these data using the effective Lagrangian approach, which consists of, in the tree approximation, the s - and u - channel nucleon, S_{11} and D_{13} exchanges, and the t -channel vector meson (ρ and ω) exchanges. The nucleon, S_{11} and vector meson exchanges have been discussed in Ref. [3] and need not be discussed in detail here. The pseudoscalar ηNN coupling constant, $g_{\eta NN}$, is taken to be 1.88, and the relevant combinations of vector meson couplings are taken to be

$$\begin{aligned}\lambda_\rho g_v^\rho + \lambda_\omega g_v^\omega &= 5.9, \\ \lambda_\rho g_t^\rho + \lambda_\omega g_t^\omega &= 17.5,\end{aligned}\tag{1}$$

where λ_i is the $V\gamma\pi$ coupling constant and g_v and g_t are the vector and tensor coupling constants to the nucleon, respectively.

For the S_{11} contribution, we take the ηN , πN and $\pi\pi N$ branching ratios to be 0.5, 0.4 and 0.1, respectively, and the total width to be 150 MeV, which are close to the preferred values found in Ref. [1]. The PDG [20] estimates the total width to be in the range from 100 to 250 MeV, and the ηN branching ratio to be between 0.35 to 0.55. In this work, we are primarily interested in the D_{13} contribution and defer discussion of the effect of these uncertainties on the determination of $A_{1/2}^s$ to a later publication. We note, however, that the quantity

$$\frac{A_{1/2}^s \sqrt{\Gamma_\eta}}{\Gamma_T}\tag{2}$$

can be determined nearly model-independently [3] from the data. Thus, to a good approximation, the effect of choosing a different width or ηN branching ratio on $A_{1/2}^s$ can be determined from (2) by an appropriate scaling. Indeed, for the results of the three fits given in Table I of Ref. [1], $A_{1/2}^s \sqrt{\Gamma_\eta}$ is nearly constant.

For the D_{13} exchange, the strong and electromagnetic effective Lagrangians are [17,21,22]:

$$L_{\eta NR} = \frac{g_R}{\mu} \bar{R}^\mu \theta_{\mu\nu}(Z) \gamma_5 N \partial^\nu \eta + \text{h.c.},\tag{3}$$

$$L_{\gamma NR}^1 = \frac{i e G_1}{2M} \bar{R}^\mu \theta_{\mu\nu}(Y) \gamma_\lambda N F^{\lambda\nu} + \text{h.c.},\tag{4}$$

$$L_{\gamma NR}^2 = -\frac{e G_2}{4M^2} \bar{R}^\mu \theta_{\mu\nu}(X) (\partial_\lambda N) F^{\nu\lambda} + \text{h.c.},\tag{5}$$

$$L_{\gamma NR}^3 = -\frac{e G_3}{4M^2} \bar{R}^\mu \theta_{\mu\nu}(V) N (\partial_\lambda F^{\nu\lambda}) + \text{h.c.},\tag{6}$$

where M is the nucleon mass, μ is the eta mass, and the tensor $\theta_{\mu\nu}(C)$ is defined as follows² [23]:

$$\theta_{\mu\nu}(C) = g_{\mu\nu} - \left[\frac{1}{2}(1 + 2C) \right] \gamma_\mu \gamma_\nu.\tag{7}$$

The gauge couplings G_i , linearly related to the D_{13} helicity amplitudes, and the off-shell parameters [23], V , X , Y , and Z , are *a priori* unknown and are determined from the fits to the data. The $\eta N D_{13}$ coupling constant, g_R , can be determined once the total width and ηN branching ratio of the D_{13} are specified. We take the total width to be 125 MeV and the ηN branching ratio to be 0.1%, that is, the D_{13} ηN partial decay width is 0.125 MeV. According to the

²We take $A = -1$ in the spin-3/2 propagator [23].

PDG [20], the D_{13} width is quite well determined, being in the range from 110 to 135 MeV. On the other hand, the ηN branching ratio is quite uncertain. It is known to be small and nonzero [4], but at this point no reasonable error can be given to it. The πN and $\pi\pi N$ branching ratios are taken to be 0.6 and 0.4, respectively.

Since the D_{13} is a $J^P=3/2^-$ state, the multipolarities of the $\gamma N D_{13}$ transition can be electric dipole (E1), magnetic quadrupole (M2) and, if the photon is virtual, Coulomb dipole (C1). The relevant resonant electroproduction multipoles are denoted by E_{2-} , M_{2-} and S_{2-} , respectively, and the transverse multipoles are related to Walker's [24] electroproduction helicity amplitudes by,

$$\begin{aligned} A_{2-} &= (3M_{2-} - E_{2-})/2, \\ B_{2-} &= M_{2-} + E_{2-}. \end{aligned} \quad (8)$$

In terms of the electroproduction transverse helicity amplitudes, the transverse helicity amplitudes in the $\gamma N D_{13}$ transition are given by,

$$\begin{aligned} A_{1/2}^d &= C \text{Im} A_{2-}, \\ A_{3/2}^d &= -\frac{\sqrt{3}}{2} C \text{Im} B_{2-}, \end{aligned} \quad (9)$$

where,

$$C = \left[\frac{4\pi q M_D \Gamma_T^2}{K_c M \Gamma_\eta} \right]^{1/2}. \quad (10)$$

Here, q is the eta three-momentum in the cm frame, M_D is the D_{13} mass (1520 MeV), Γ_T the total D_{13} width, Γ_η is the $D_{13} \rightarrow \eta N$ partial decay width, and $K_c = (W^2 - M^2)/(2W)$ is the equivalent real photon energy in the cm frame. All quantities are to be evaluated at $W = M_D$. For the Coulomb (or scalar) transition, we have

$$S_{1/2}^d = \sqrt{\frac{2Q^2}{k^2}} C \text{Im} S_{2-}, \quad (11)$$

again evaluated at $W = M_D$. Here, k is the three-momentum of the virtual photon in the cm frame.

The parameters of the model are $g_{\eta NN}$, two combinations of the vector meson couplings, the helicity amplitudes $A_{1/2}^s$ and $S_{1/2}^s$, the helicity amplitudes $A_{1/2}^d$, $A_{3/2}^d$, and $S_{1/2}^d$, and the four off-shell parameters, for a total of 12 parameters. The background is predominantly s- and p-wave, and controlled by $g_{\eta NN}$, the vector meson couplings and the off-shell parameters. As there are tremendous correlations amongst these parameters, we hold $g_{\eta NN}$ and the vector meson couplings fixed at the values given above and allow the off-shell parameters to vary in the fits. As this is done at each Q^2 , the fitted off-shell parameters can largely compensate for any bias introduced by our choices of the vector meson couplings and $g_{\eta NN}$.

As the data have practically no angular dependence and the experiment was performed only at one ϵ , the polarization of the virtual photon, no separation of $A_{1/2}^s$ and $S_{1/2}^s$ is possible. The reason for this is that in the differential cross section, there is no interference term between the E_{0+} and S_{0+} multipoles³, and therefore, some arbitrary linear combination of these two would lead to an angular-independent differential cross section. At lower Q^2 , a transverse-longitudinal separation was made [25] and it was found the the longitudinal cross section is small compared to the transverse one. We assume that this continues to higher Q^2 , and do fits with $S_{1/2}^s$ fixed either at zero or roughly⁴ 10% of $A_{1/2}^s$.

Thus, the parameters to be fitted to the data [1] are $A_{1/2}^s$, the three helicity amplitudes for the D_{13} , and the four off-shell parameters, for a total of eight parameters. The results of various fits are given in Table 1 for both $Q^2 = 2.4$ GeV² and $Q^2 = 3.6$ GeV². We use the CERN routine MINUIT to minimize the chi-squared and the errors on the parameters are the so-called MINOS errors, which accounts for correlations amongst the parameters. In all cases, the fit to the data is excellent. In the first fit, we have fixed $S_{1/2}^s$ at roughly 10% of $A_{1/2}^s$ and allowed $A_{1/2}^s$ and the D_{13}

³The E_{0+} multipole is $\sim A_{1/2}^s$, while the S_{0+} multipole is $\sim S_{1/2}^s$ [17].

⁴Specifically, since we don't expect our result for $A_{1/2}^s$ to be much different than found in Ref. [1], we fix $S_{1/2}^s$ to be 10% of $A_{1/2}^s$ found in that work.

parameters (the three helicity parameters and the off-shell parameters) to vary. The extracted $A_{1/2}^s$ is in excellent agreement with that found in [1]. At $Q^2 = 2.4 \text{ GeV}^2$, the extracted helicity amplitudes of the D_{13} all have extremely large errors and are consistent with zero. This is consistent with the statement made in Ref. [1] that the data are angular independent at the one-sigma level. At $Q^2 = 3.6 \text{ GeV}^2$, there is a slight signal for the presence of the D_{13} . To examine the role of the D_{13} in the fit, we have turned off the D_{13} and refitted $A_{1/2}^s$ keeping $S_{1/2}^s$ fixed at roughly 10 % of $A_{1/2}^s$. At both $Q^2 = 2.4$ and 3.6 GeV^2 , the chi-squared per degree of freedom, χ^2/dof , *increases*, but not significantly. $A_{1/2}^s$ shifts slightly upward, but within error is in agreement with that obtained from the first fit. In a final fit, we examined the role of $S_{1/2}^s$ by setting it zero and refitting $A_{1/2}^s$ and the D_{13} parameters. The results turn out to be quite close to the fit with $S_{1/2}^s$ fixed at 10% of $A_{1/2}^s$.

To summarize our numerical results obtained from the differential cross section, we find $A_{1/2}^s$ to be $50 \pm 4 \times 10^{-3} \text{ GeV}^{-1/2}$ at 2.4 GeV^2 and 35 ± 2 at 3.6 GeV^2 , in the same units. The errors here do not take into account uncertainties in the branching ratio, total width and mass of the S_{11} , which were studied in Ref. [1]. Our errors are dominated by uncertainties in the D_{13} contribution, and thus should be added to the errors found in Ref. [1]. Our results for $A_{1/2}^s$ are in excellent agreement with those found in Ref. [1]. At first thought, this may come as no surprise since we have used values for the total width and ηN branching ratio close to their preferred values. However, it should be emphasized that our method of analysis is quite different than the one used in [1]. In that work, the cross section was written as an incoherent sum of a resonance contribution and a background contribution, and it was found that the background contribution was less than 1% of the resonant contribution. In our work, we have a coherent sum of the resonance and background, and find that the background contributes at the 10% level or more. In addition, the role of the D_{13} was ignored in Ref. [1].

At a W of 1.54 GeV , our results are graphically⁵ depicted in Fig. 1 at 2.4 GeV^2 , and in Fig. 2 at 3.6 GeV^2 . The solid line is the result of the first fit, while the dashed-line arises when the D_{13} is turned off, everything else held fixed. These two lines are distinctly different and the data do seem to favor the solid line, which contains the D_{13} . However, to gauge the *need* for the D_{13} , one should compare with the results of the second fit, that is, with the D_{13} turned off and $A_{1/2}^s$ refitted to the data. This is shown by the dotted lines in Figs. 1 and 2. Looking at the graphs, it is difficult to tell if the data favor the solid or dotted line. At angles where most of the data exist, the dotted line is roughly the average of the solid line. However, at $Q^2 = 2.4 \text{ GeV}^2$ and $\phi = 90^\circ$, the solid and dotted lines are quite different. Therefore, data at this angle would help pin down the D_{13} parameters.

There are two main reasons that the current data do not tightly constrain the D_{13} helicity amplitudes, in contrast to what happens at the real photon point [4]. First, the D_{13} is falling faster than the S_{11} as a function of Q^2 , and thus is simply less important at these Q^2 values than at $Q^2 = 0$. Second, the key to pinning down the D_{13} helicity amplitudes at the real photon point is the new polarization observables in conjunction with the differential cross section data. At present, similar polarization observables do not exist for electroproduction. However, an experiment has recently been completed [19] at the J-Lab, which should have significant bearing on the extraction of the D_{13} helicity amplitudes from the eta electroproduction data.

In the J-Lab experiment [19], the data of which are now in the preliminary stages of analysis, both the beam and target were longitudinally polarized, i.e., parallel or anti-parallel to the beam direction. The polarization of the target was periodically flipped, resulting in the measurement of an asymmetry, which we denote as:

$$A_{et}^+ = \frac{\sigma(h = 1, p = 1) - \sigma(h = 1, p = -1)}{\sigma(h = 1, p = 1) + \sigma(h = 1, p = -1)}, \quad (12)$$

where h is the helicity of the incoming electron and p is the polarization of the target with \hat{z} *defined to be in the direction of the incident electron beam*. Following Ref. [26], but correcting some mistakes originally pointed out by Dmitrasinovic *et al.* [27], the differential cross section for the case of polarized beam and target can be written as

$$\sigma(\theta, \phi) = \sigma_0 + \sigma_e + \sigma_t + \sigma_{et}. \quad (13)$$

The expression for the unpolarized cross section, σ_0 , has a standard form and will not be given here. For the other contributions, we work with the transverse helicity amplitudes, h_{\pm}^i , which are related to those of Walker [24] by

$$h_{\pm}^N = (H_4 \pm H_1)/\sqrt{2}, \quad (14)$$

$$h_{\pm}^F = (H_3 \mp H_1)/\sqrt{2}. \quad (15)$$

⁵The data shown in Figs. 1 and 2 represent only a small fraction of the data [1] used in our fit.

Walker's H_i are in turn related to the CGLN [28] \mathcal{F} 's by

$$H_1(\theta) = -\frac{1}{\sqrt{2}} \sin \theta \cos(\theta/2) [\mathcal{F}_3 + \mathcal{F}_4] \quad (16)$$

$$H_2(\theta) = \sqrt{2} \cos(\theta/2) \left[\mathcal{F}_2 - \mathcal{F}_1 + \frac{1}{2}(1 - \cos \theta)(\mathcal{F}_3 - \mathcal{F}_4) \right] \quad (17)$$

$$H_3(\theta) = \frac{1}{\sqrt{2}} \sin \theta \sin(\theta/2) [\mathcal{F}_3 - \mathcal{F}_4] \quad (18)$$

$$H_4(\theta) = \sqrt{2} \sin(\theta/2) \left[\mathcal{F}_2 + \mathcal{F}_1 + \frac{1}{2}(1 + \cos \theta)(\mathcal{F}_3 + \mathcal{F}_4) \right]. \quad (19)$$

The longitudinal helicity amplitudes, h_0^i , are related to the CGLN [29] \mathcal{F} 's by

$$h_0^N = -\sqrt{\frac{-K^2}{k^2}} (\mathcal{F}_7 + \mathcal{F}_8) \cos(\theta/2), \quad (20)$$

$$h_0^F = \sqrt{\frac{-K^2}{k^2}} (\mathcal{F}_7 - \mathcal{F}_8) \sin(\theta/2). \quad (21)$$

Comparing with Ref. [30], our $\mathcal{F}_{1,2,3,4}$ are the same as their's, and our $\mathcal{F}_{7,8}$ are related to their $\mathcal{F}_{5,6}$ by,

$$k_0 \mathcal{F}_7 = k \mathcal{F}_6, \quad (22)$$

$$k_0 \mathcal{F}_8 = k \mathcal{F}_5, \quad (23)$$

where k_0 is the energy of the virtual photon in the cm frame.

For a polarized beam, σ_e enters the cross section, and is given by,

$$\begin{aligned} \sigma_e &= h \frac{q}{K_c} \sqrt{2\epsilon(1-\epsilon)} \sin(\phi) \text{Im}(h_0^N h_-^{*N} + h_0^F h_-^{*F}), \\ &= h f_e \end{aligned} \quad (24)$$

For a polarized target, σ_t enters and is given by

$$\begin{aligned} \sigma_t &= \frac{q}{K_c} \left[P_x (\sqrt{2\epsilon(1+\epsilon)} \sin(\phi) \text{Im} X_1 + \epsilon \sin(2\phi) \text{Im} X_2) \right. \\ &\quad - P_y (\text{Im} Y_1 + \epsilon \cos(2\phi) \text{Im} Y_2 + 2\epsilon \text{Im} Y_3 + \sqrt{2\epsilon(1+\epsilon)} \cos(\phi) \text{Im} Y_4) \\ &\quad \left. - P_z (\epsilon \sin(2\phi) \text{Im} Z_2 + \sqrt{2\epsilon(1+\epsilon)} \sin(\phi) \text{Im} Z_1) \right], \\ &= P_x f_{tx} - P_y f_{ty} - P_z f_{tz}, \end{aligned} \quad (25)$$

where

$$\begin{aligned} X_1 &= h_0^F h_+^{*N} + h_0^N h_+^{*F} & X_2 &= h_-^F h_+^{*N} + h_-^N h_+^{*F} \\ Y_1 &= h_+^N h_+^{*F} + h_-^N h_-^{*F} & Y_2 &= h_-^N h_-^{*F} - h_+^N h_+^{*F} \\ Y_3 &= h_0^N h_0^{*F} & Y_4 &= h_0^N h_-^{*F} - h_0^F h_-^{*N} \\ Z_1 &= h_0^N h_+^{*N} - h_0^F h_+^{*F} & Z_2 &= h_-^N h_+^{*N} - h_-^F h_+^{*F}. \end{aligned} \quad (26)$$

If both beam and target are polarized, σ_{et} also enters:

$$\begin{aligned} \sigma_{et} &= h \frac{q}{K_c} \left[P_x (\sqrt{2\epsilon(1-\epsilon)} \cos(\phi) \text{Re} X_1 + \sqrt{1-\epsilon^2} \text{Re} X_2) \right. \\ &\quad + P_y \sqrt{2\epsilon(1-\epsilon)} \sin(\phi) \text{Re} Y_4 \\ &\quad \left. - P_z (\sqrt{1-\epsilon^2} \text{Re} Z_2 + \sqrt{2\epsilon(1-\epsilon)} \cos(\phi) \text{Re} Z_1) \right], \\ &= h (P_x f_{etx} + P_y f_{ety} - P_z f_{etz}). \end{aligned} \quad (27)$$

The P_i in (25,27) are defined in a frame in which \hat{z} is in the direction of the virtual photon, \hat{y} is in the direction of $\vec{k} \times \vec{q}$, and \hat{x} is in the direction of $\vec{y} \times \vec{z}$. Here, \vec{k} is the three-momentum of the virtual photon and \vec{q} is the

three-momentum of the eta, both in the cm frame. If the target is 100% polarized in the beam direction, then we find that the relevant P_i to be used in (25,27) are

$$P_z = \cos \beta \quad P_x = \sin \beta \cos \phi \quad P_y = -\sin \beta \sin \phi, \quad (28)$$

where β is the angle between the incident beam and the direction of the virtual photon;

$$\cos \beta = \frac{\nu + Q^2/(2E)}{\sqrt{\nu^2 + Q^2}}, \quad (29)$$

with E the lab beam energy and ν the energy of the virtual photon in the lab frame. For the J-Lab experiment, we find A_{et}^+ becomes

$$A_{et}^+ = \frac{P_x(f_{tx} + f_{etx}) + P_y(f_{ety} - f_{ty}) - P_z(f_{tz} + f_{etz})}{\sigma_0 + f_e}, \quad (30)$$

with the P_i given in (28).

For the case of a pure E_{0+} amplitude, i.e., total S_{11} dominance, one obtains the simple result

$$A_{et}^+ = -\cos \beta \sqrt{1 - \epsilon^2}, \quad (31)$$

which is obviously independent of θ and ϕ . For the differential cross-section, it is difficult to isolate the D_{13} since, with the current statistics, a rescaling of the E_{0+} can mimic (within the error bars) the effect of the D_{13} . On the other hand, for A_{et}^+ a scaling of E_{0+} essentially leaves this observable unchanged. Therefore, this observable should be able to distinguish between the fits with and without the D_{13} . This is verified, as is shown in Fig. 3. The solid line is the fit with the D_{13} , while the dashed line is this fit with the D_{13} turned off. The dotted line, which lies practically on top of the dashed line, is the best fit without the D_{13} . Thus, we see that this observable is very sensitive to the D_{13} and should provide powerful constraints on its helicity amplitudes.

In summary, we have investigated the role of the D_{13} in various eta electroproduction observables, which are readily measurable, for example, in Hall B at J-Lab. The signal for the D_{13} contribution is very weak in the present differential cross section data. A full 4π coverage of the differential cross section should show increased sensitivity to the D_{13} . Even stronger constraints on the D_{13} should be provided by the asymmetry A_{et}^+ , discussed above, which has been recently measured at J-Lab. Regarding the S_{11} , we confirm the results of Ref. [1], but the errors in that work should be increased slightly due to uncertainties in the D_{13} sector. Finally, a tranverse-longitudinal separation would be useful as the Q^2 dependences of the longitudinal amplitudes are also of interest as tests of QCD-inspired models, and of QCD itself.

We are grateful to C. Armstrong and P. Stoler for providing us their results on eta electroproduction prior to publication. We also thank P. Stoler for a critical reading of this manuscript. Our research is supported by the U. S. Department of Energy.

- [1] C. Armstrong *et al.*, Phys. Rev. D, **60**, 052004 (1999).
- [2] V. Frolov, *et al.*, Phys. Rev. Lett. **82**, 45 (1999).
- [3] M. Benmerrouche, N.C. Mukhopadhyay and J.F. Zhang, Phys. Rev. D **51**, 3237 (1995).
- [4] Nimai C. Mukhopadhyay and Nilmani Mathur, Phys. Lett. **B444**, 7 (1998).
- [5] V. Burkert, in *Exicted Baryons 1988*, G. Adams, N.C. Mukhopadhyay and P. Stoler, eds., (World Scientific, Teaneck, N.J. 1989).
- [6] P. Stoler, Phys. Rep. **226**, 103 (1993).
- [7] C. E. Carlson, Phys. Rev. D **34**, 2704 (1986).
- [8] L.A. Copley, G. Karl and E. Obryk, Phys. Lett. **B29**, 117 (1969). S. Ono, Nucl. Phys. **B107**, 522 (1976).
- [9] See, for example, the contributions by A.V. Radyushkin (p. 366) and C. Carlson (p. 376) in, *Baryon '92*, Moshe Gai, ed. (World Scientific, Singapore, 1993).
- [10] N. Isgur and G. Karl, Phys. Lett. **B72**, 109 (1977); *ibid.*, **B74**, 353 (1978).
- [11] W.N. Cottingham and I.H. Dunbar, Z. Phys. **C2**, 41 (1979). H. Breuker *et al.*, Z. Phys. **C17**, 121 (1983). V. Burkert and Zh. Li, CEBAF proposal PR-92-017 (1992).

- [12] S. Capstick and W. Roberts, Phys. Rev. D **49**, 4570 (1994).
[13] L. Ya. Glozman and D.O. Riska, Phys. Rep. **268**, 263 (1996).
[14] S. Capstick and B.D. Keister, Phys. Rev. D **51**, 3598 (1995). W. Konen and H.J. Weber, Phys. Rev. D **41**, 2201 (1990).
[15] C.E. Carlson, C.D. Carone, J.L. Goity and R.F. Lebed, Phys. Rev. D **59**, 114008 (1999).
[16] U. Beck *et al.*, Phys. Lett. **B51**, 103 (1974). J.C. Adler *et al.*, Nucl. Phys. **B91**, 386 (1975). I.I. Breuker *et al.*, Phys. Lett. **B74**, 409 (1978). F.W. Brasse *et al.*, Z. Phys. **C22**, 33 (1984).
[17] M. Benmerrouche, N.C. Mukhopadhyay and J.F. Zhang, Phys. Rev. Lett. **77**, 4716 (1996).
[18] A. Bock *et al.*, Phys. Rev. Lett. **81**, 537 (1998). J. Ajaka *et al.*, Phys. Rev. Lett. **81**, 1797 (1998). B. Krusche, *et al.*, Phys. Rev. Lett. **75**, 3736 (1995); Phys. Lett. **B358**, 40 (1995).
[19] CEBAF Hall B proposal, *Study of the $\Delta(1232)$ Using Double Polarization Asymmetries*, P. Stoler, contact person. Data taking for this experiment has been completed and the raw data are now being analyzed, P. Stoler, private communication (1999).
[20] C. Caso *et al.*, Particle Data Group, Eur. Phys. J. **C3**, 1 (1998).
[21] R.M. Davidson, N.C. Mukhopadhyay and R.S. Wittman, Phys. Rev. D **43**, 71 (1991).
[22] R.M. Davidson, Few-Body Systems, Suppl. **11**, 140 (1999).
[23] M. Benmerrouche, R.M. Davidson and N.C. Mukhopadhyay, Phys. Rev. C **39**, 2239 (1989).
[24] R.L. Walker, Phys. Rev. **182**, 1729 (1969).
[25] H. Breuker *et al.*, Phys. Lett. **B74**, 409 (1978). F. Brasse *et al.*, Nucl. Phys. **B139**, 37 (1978).
[26] A. Bartl and W. Majerotto, Nucl. Phys. **B62**, 267 (1975).
[27] V. Dmitrasinovic, T.W. Donnelly, and F. Gross, proceedings of *CEBAF 1987 Summer Study Group*, 547 (1988).
[28] G.F. Chew, M.L. Goldberger, F.E. Low, and Y. Nambu, Phys. Rev. **106**, 1345 (1957).
[29] A. Donnachie, in *Photo- and Electroproduction*, High Energy Physics, vol. 5 (E.H.S. Burhop, ed., Academic Press, New York) 1972.
[30] G. Knöchlein, D. Drechsel, and L. Tiator, Z. Phys. **A352**, 327 (1995).

TABLE I. The helicity amplitudes extracted from the data [1] using our effective Lagrangian approach. At each Q^2 , the first row gives the results when $A_{1/2}^s$ and the D_{13} parameters are allowed to vary with $S_{1/2}^s$ fixed at roughly 10% of $A_{1/2}^s$. The second row shows the best fit with the D_{13} turned off. The last row shows the best fit under the assumption $S_{1/2}^s = 0$.

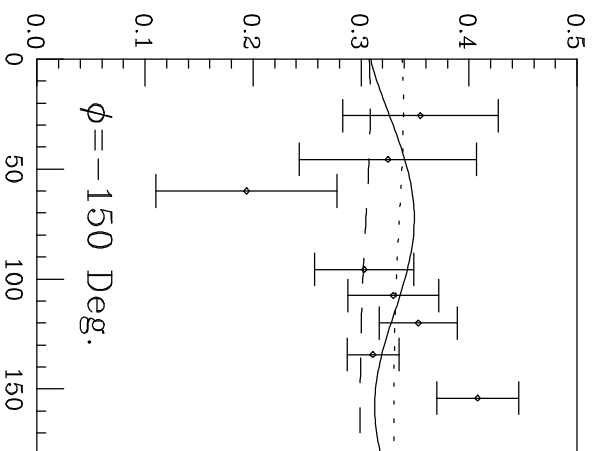
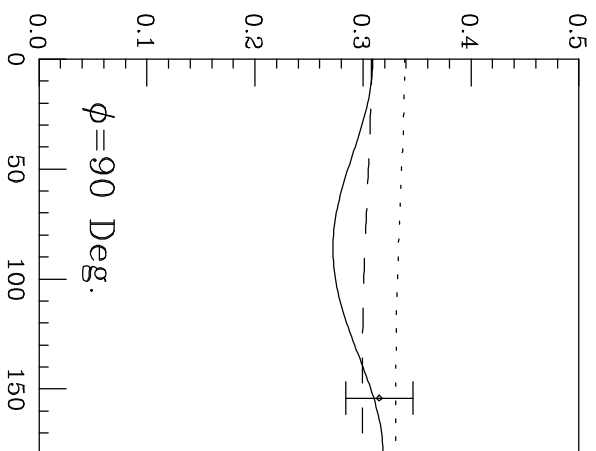
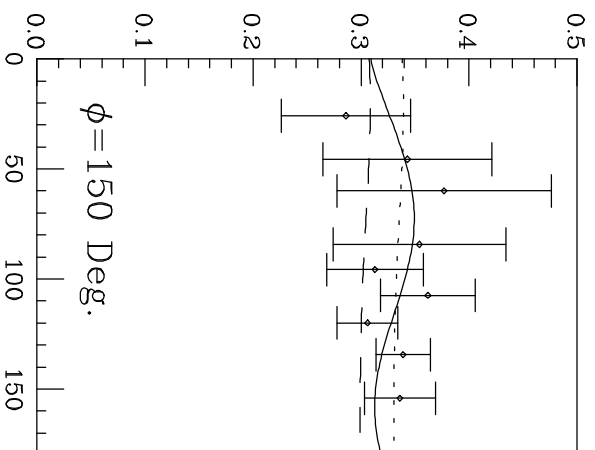
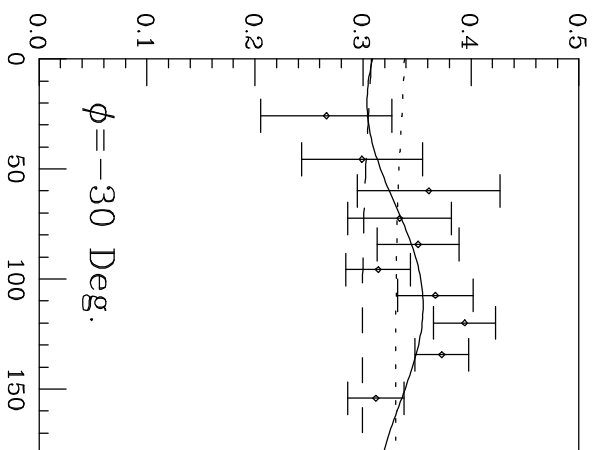
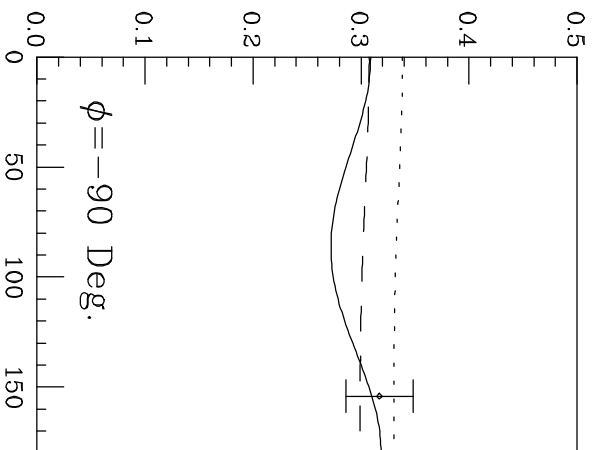
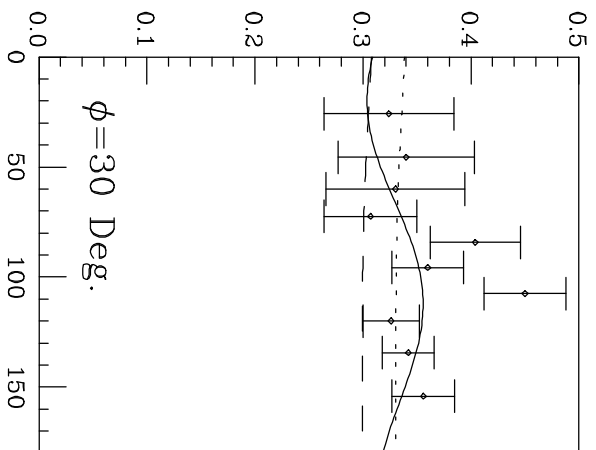
Q^2 GeV ²	$N^*(1535)$		$N^*(1520)$			χ^2/dof
	$A_{1/2}^s$	$S_{1/2}^s$	$A_{1/2}^d$	$A_{3/2}^d$	$S_{1/2}^d$	
2.4	49 ± 2	5.0	-2 ± 66	96 ± 99	24 ± 91	0.80
	51.5 ± 0.3	5.0	0.0	0.0	0.0	0.88
	49.5 ± 3.5	0.0	5 ± 76	84 ± 113	19 ± 102	0.80
3.6	34 ± 1	3.5	18 ± 8	5 ± 11	-13 ± 9	0.79
	36.7 ± 0.2	3.5	0.0	0.0	0.0	0.87
	35 ± 1	0.0	18 ± 6	0 ± 5	-14 ± 8	0.79

FIG. 1. Comparison of our fits to the J-Lab data [1] at $W = 1.54$ GeV and $Q^2 = 2.4$ GeV². Solid line is the fit where the D_{13} parameters vary and it is assumed $(S_{1/2}^s)/(A_{1/2}^s) \approx 10\%$. The dashed-line is obtained from this fit when the D_{13} is turned off, everything else held fixed. The dotted line is the best fit without the D_{13} .

FIG. 2. Comparison of our fits to the J-Lab data [1] at $W = 1.54$ GeV and $Q^2 = 3.6$ GeV². Curves as in Fig. 1.

FIG. 3. Predictions for A_{et}^+ , defined in the text, at $W = 1.54$ GeV based on fits to the differential cross section. Curves as in Fig. 1.

$d\sigma/d\Omega$ ($\mu\text{b}/\text{Sr}$)



Θ (Deg.)

$d\sigma/d\Omega$ ($\mu\text{b}/\text{Sr}$)

